Entanglement resonance in the asymmetric quantum Rabi model

Yu-Qing Shi,[1,2] Lei Cong,[3,4,5,*] and Hans-Peter Eckle[6,†]

[1]*School of Physical Science and Technology, Lanzhou University, Lanzhou 730000, China*
[2]*Key Laboratory for Electronic Materials, College of Electrical Engineering, Northwest Minzu University, Lanzhou 730030, China*
[3]*International Center of Quantum Artificial Intelligence for Science and Technology (QuArtist) and Department of Physics, Shanghai University, 200444 Shanghai, China*
[4]*Helmholtz-Institut, GSI Helmholtzzentrum fur Schwerionenforschung, Mainz 55128, Germany*
[5]*Department of Applied Physics, Nanjing Tech University, Nanjing 210009, China*
[6]*Humboldt Study Centre, Ulm University, Ulm D-89069, Germany*

(Received 19 October 2021; revised 29 March 2022; accepted 8 June 2022; published 27 June 2022)

We investigate the entanglement features in the interacting system of a quantized optical field and a two-level system which is statically driven, known as the asymmetric quantum Rabi model (AsymQRM). Intriguing entanglement resonance valleys with the increase of the photon-atom coupling strength and peaks with the increase of the driving amplitude are found. It is revealed that both of these two kinds of entanglement resonance are caused by the avoided level crossing of the associated eigenenergies. In sharp contrast to the quantum Rabi model, the entanglement of the AsymQRM collapses to zero in the strong coupling regime except when the driving amplitude is equal to $m\omega/2$, with m being an integer and ω being the photon frequency. Our analysis demonstrates that such entanglement reappearance is induced by the hidden symmetry of the AsymQRM. Supplying an insightful understanding of the AsymQRM, our results will be helpful in exploring the hidden symmetry and in preparing photon-atom entanglement in light-matter coupled systems.

DOI: 10.1103/PhysRevA.105.062450

I. INTRODUCTION

Light-matter interaction is described by coupling bosonic and fermionic subsystems. Modeling the interaction between bosonic modes and the electrons of atomic levels plays therefore a fundamental role in the physics of strongly interacting quantum systems [1], especially, but not exclusively, in models related to quantum optics [2].

For instance, *resonance phenomena* of optical systems where the frequency of a single-mode (bosonic) radiation field is such that it couples approximately only to two relevant atomic levels, i.e., a two-level system (TLS) or qubit (see below for this latter designation), have attracted considerable interest for many years [3] and continue to do so, as evidenced in many recent publications, a pertinent selection of which we are going to reference in this paper, especially its introduction. The two-level system can be described also by spin degrees of freedom.

While the semiclassical treatment of such systems [4] by Rabi initiated the study of the eponymous model, the quantum version, introduced by Jaynes and Cummings [5] (for more details on the quantum Rabi model (QRM), see, e.g., Ref. [6]), has attracted considerable recent interest. A theoretical breakthrough was achieved by the exact solution of the QRM [7,8] using two different methods, which, however, both crucially used the $\mathbb{Z}_2$ symmetry of the QRM and a Bargmann space analysis (for these and further recent theoretical developments, see Refs. [9–11], and for recent reviews, see Refs. [12–16]).

The QRM has been realized experimentally in solid state devices, in physical systems including cavity quantum electrodynamic (cavity-QED) [1] and circuit quantum electrodynamic (circuit-QED) [17] systems, and also in trapped ion systems [18,19].

In recent years, it became possible, triggered by the technological possibilities these and further experimental systems have opened up, to tune the parameters of the QRM, in particular, to reach new regimes where the interaction between the bosonic modes and the TLS is strong, i.e., to reach the so-called ultrastrong (where the ratio of the field-TLS coupling strength g and the field frequency ω is between 0.1 and 1) [20–23] and even the so-called deep strong ($g/\omega > 1$) coupling regimes, predicted theoretically [24] and realized experimentally in photonic systems [25]. Through these developments the necessity arose to consider fully the QRM (for a recent review, see Ref. [26]) instead of the simpler quantum Jaynes-Cummings model which is obtained from the QRM by applying the rotating wave approximation (RWA) [5].

Further intriguing developments include the theoretical prediction of a few-body quantum phase transition in the QRM [27,28], which has subsequently been observed experimentally in a single trapped ion [19], excited-state quantum phase transitions [29] and quantum phase transitions in extensions of the QRM that include symmetry breaking terms, the focal point of the present study, and nonlinear interac-

*congllzu@gmail.com
†hans-peter.eckle@uni-ulm.de

tion terms [30], and the application of the QRM in quantum metrology [31].

Recently, systems related to the QRM have been studied especially in connection with quantum computing [32–34], where the fundamental building units (qubits) are two-level systems. Moreover, many physically interesting generalizations of the QRM have been examined (for a recent review of the theoretical developments in this area, see Ref. [13]).

In this paper, we shall especially consider the asymmetric extension of the QRM (AsymQRM) [7], where a $\mathbb{Z}_2$ symmetry breaking term, a driving term, $\epsilon\sigma_x$, is added to the Hamiltonian of the QRM. Other than in cavity-QED systems, such a term arises naturally in the solid state devices mentioned earlier [20–23]. The AsymQRM has earlier been proposed for experimental realization in a micromechanical resonator coupled to a Cooper-pair box [35,36].

The AsymQRM is of great theoretical importance, especially because the broken $\mathbb{Z}_2$ symmetry is restored for particular values of the driving amplitude ϵ [7] and is currently positioned at the center of the fundamental quest for a characterization of integrability in the quantum regime [37].

Before we return to the focus of this paper, the asymmetric QRM, we mention in passing one of the numerous other extensions of the QRM that are currently under intense investigation and which originated in a suggestion for an experimental arrangement creating a nonlinear interaction between the bosonic modes and the TLS [38]. This so-called Stark term, $\gamma\sigma_z a^\dagger a$, preserves the $\mathbb{Z}_2$ symmetry of the QRM and has also been rigorously solved using a Bargmann representation [39–41], and its physical properties have been further investigated [42]. This model is also discussed as a promising candidate for another foray to shed light on the fundamental notion of quantum integrability [43]. The reason for this expectation is that, within the rotating wave approximation, the quantum Jaynes-Cummings model admits an exact solution using the infinite Lie algebra approach of the Richardson-Gaudin-type Bethe ansatz [44–46] while adding a nonlinear Stark term $\gamma a^\dagger a\sigma_z$ renders the quantum Jaynes-Cummings-Stark model amenable to an algebraic Bethe ansatz and the model is thus a Yang-Baxter integrable model [46,47].

Another intriguing development, with promising applications to other physical systems, the anisotropic QRM, interpolating between the quantum Jaynes-Cummings model and the full QRM [48,49], can be extended to the quantum Rabi-Stark model (QRSM) [50,51]. Furthermore, asymmetric models have been discussed where the asymmetry term does not break the $\mathbb{Z}_2$ symmetry [52]. Lastly, we mention the polaron picture [53,54], which has been successfully applied to investigate the two-photon [55] and two-qubit [56] QRM.

Currently, the QRM and its many variants are also discussed in connection with the fundamental question of quantum entanglement [57,58], which reflects the nonlocal nature of quantum physics and is thus a basic resource of quantum technology. Quantum entanglement, on the other hand, is again at the root of such promising technological developments as quantum computation, quantum information [32–34], which we have already mentioned above, and quantum communication [59].

The present study adds to these developments, especially their theoretical side, by studying numerically the phenomenon of *quantum entanglement resonance* in the asymmetric quantum Rabi model (AsymQRM). We address, in particular, how the physical quantity of entanglement entropy can be used to distinguish level crossings from (narrowly) avoided level crossings. This distinction is of central importance in the study of the hidden symmetry of the asymmetric QRM [7,60–67], where the $\mathbb{Z}_2$ symmetry, and hence level crossings, are restored for half-integer values of the amplitude of the driving term ϵ in units of the field strength ω. In order to address this distinction, the numerical accuracy with which spectra can be calculated is often insufficient to decide clearly between these two cases, true level crossings and narrowly avoided level crossings. The entanglement entropy offers a more sensitive way to distinguish level crossings from avoided level crossings because it uses not only the eigenvalues but also the (low-lying) eigenstates of the Schrödinger equation of the AsymQRM. Studying the von Neumann entanglement entropy (for other entanglement entropy notions, see, e.g., Ref. [68]) of the eigenstates of the asymmetric QRM for different coupling strengths g and driving amplitudes ϵ, we find that the entropy is sensitive to the spectral structure, exhibiting distinctive resonance valleys when the coupling strength g is increased and resonance peaks when the driving amplitude ϵ is increased. These resonances occur in both cases at the loci of the avoided level crossings of the energy spectra.

We note that entanglement entropy has already been used in the study of level crossings in the anisotropic QRM [48] and the spectral classification of coupling regimes [69], as well as the QRM in the polaron picture [70]. Moreover, similar entanglement resonance behavior has been discussed earlier in quantum spin chains [71] and periodically driven multipartite quantum systems [72].

In Sec. II of this paper, we give the Hamiltonian and the entanglement characterization of the AsymQRM. The entanglement resonance with the increase of the photon-atom coupling strength is also revealed. In Sec. III, we study the entanglement resonance with the increase of the driving amplitude. The entanglement preservation caused by the hidden symmetry is also uncovered. Finally, we give a summary in Sec. IV. In the Appendix, we provide some physical intuition for the entanglement entropy of the simpler asymmetric quantum Jaynes-Cummings model, where analytical calculations are feasible to a much greater extent than in the asymmetric quantum Rabi model.

II. ENTANGLEMENT RESONANCE

The AsymQRM describes the interaction between a quantized bosonic field and a two-level system and is subject to a static-field-driven two-level atom with Hamiltonian

$$\hat{H} = \omega_0\hat{\sigma}_+\hat{\sigma}_- + \omega\hat{a}^\dagger\hat{a} + [g(\hat{a}^\dagger + \hat{a}) + \epsilon](\hat{\sigma}_+ + \hat{\sigma}_-), \quad (1)$$

acting in the tensor Hilbert space $\mathcal{H}_a \otimes \mathcal{H}_f$, where $\hat{a}$ and $\hat{a}^\dagger$ are the bosonic annihilation and creation operators acting in the Hilbert space $\mathcal{H}_f$ with frequency ω, $\hat{\sigma}_+ = \hat{\sigma}_-^\dagger = |e\rangle\langle g|$ are the transition operators between the ground state $|g\rangle$ and the excited state $|e\rangle$ acting in the two-dimensional Hilbert space

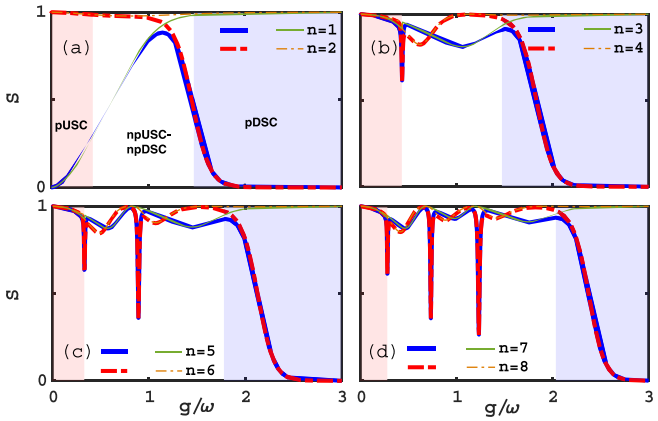

FIG. 1. Entanglement entropy of different eigenstates $|\Psi_n\rangle$ of the AsymQRM with $\epsilon = 0.01\omega$ denoted by thick lines when $n = 1, 2$ in (a), 3,4 in (b), 5,6 in (c), and 7,8 in (d) as a function of atom-field coupling strength g. The corresponding thin lines denote the results of QRM with $\epsilon = 0$. Different background colors from left to right denote the pUSC, the npUSC-npDSC, and the pDSC regimes, respectively. We use $\omega_0 = \omega$. The truncation number in the numerical calculation is 400.

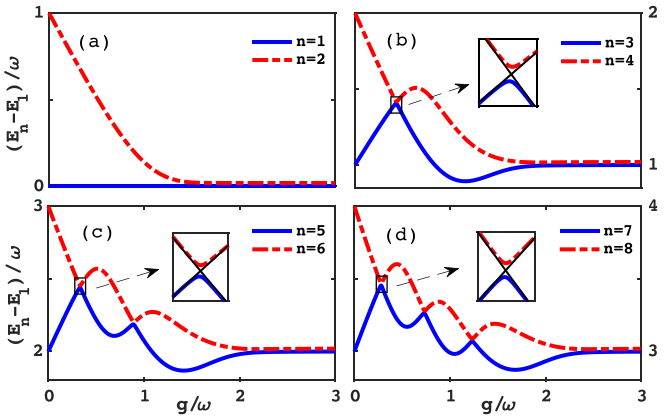

FIG. 2. (a)–(d) Eigenenergies corresponding to the AsymQRM in Fig. 1 relative to the ground-state energy E_1. The thin solid lines in each inset which cross each other are the eigenenergies of the QRM with $\epsilon = 0$. The coupling values of g of entanglement resonances in the npUSC-npDSC regime in Fig. 1 exactly match the ones at which the associated eigenenergies show avoided level crossings. The truncation number in the numerical calculation is again 400.

$\mathcal{H}_a$ of the two-level atom with frequency ω_0, g is the atom-field coupling strength, and ϵ is the amplitude of static driving.

The atom-field entanglement of any eigenstate $|\Psi_n\rangle$ of the AsymQRM can be quantified by the entanglement entropy, which we choose here as the von Neumann entropy of the reduced density matrix for any one of the subsystems [58], e.g., the field (f) and atomic (a) subsystems considered here,

$$S = -\mathrm{Tr}(\rho_\mathrm{a}\log_2\rho_\mathrm{a}) = -\mathrm{Tr}(\rho_\mathrm{f}\log_2\rho_\mathrm{f}), \tag{2}$$

where $\rho_\mathrm{a} = \mathrm{Tr}_\mathrm{f}(|\Psi_n\rangle\langle\Psi_n|)$ and $\rho_\mathrm{f} = \mathrm{Tr}_\mathrm{a}(|\Psi_n\rangle\langle\Psi_n|)$. The entanglement entropy vanishes for a separable state and equals 1 for a maximally entangled state.

The Hamiltonian (1) has no obvious symmetry. Therefore the eigenstates $|\Psi_n\rangle$ can only be labeled by the energy eigenvalues E_n of the Schrödinger equation

$$H|\Psi_n\rangle = E_n|\Psi_n\rangle. \tag{3}$$

We numerically evaluate the entropy expressions (2) by expanding the Hamiltonian (1) in the complete basis $|m, p\rangle = |m\rangle|p\rangle$, $m = 0, 1, 2, \ldots$, $p = \pm$ of the combined system of the atom and the field

$$|\Psi_n\rangle = \sum_{m,p} c_{m,p}^{(n)}|m, p\rangle \tag{4}$$

to obtain the matrix representation of the Hamiltonian (1), which we use to numerically obtain eigenvalues and eigenstates in a truncated Hilbert space at a photon number $n = n_\mathrm{trunc}$ such that the obtained magnitudes of the eigenenergies converge.

We present in Fig. 1 the entanglement entropy of different eigenstates $|\Psi_n\rangle$ of the AsymQRM and the QRM Hamiltonian, respectively, as a function of the atom-field coupling strength g. According to the classification rule proposed in Ref. [69] for $\epsilon = 0$, the coupling regimes of both the QRM and the AsymQRM can be divided into three regions, the perturbative ultrastrong coupling (pUSC) regime, the perturbative deep strong coupling (pDSC) regime, and the intermediate region, designated as the nonperturbative ultrastrong–deep strong coupling (npUSC-npDSC) regime. The regimes pUSC and npUSC-npDSC are separated by the first energy-level crossing point, and the npUSC-npDSC and pDSC regimes are separated by the energy-level coalescence point, where the adjacent eigenenergies become quasidegenerate.

This spectral classification is based on the validity of perturbative criteria of the quantum Rabi model, which allows the use of exactly solvable effective Hamiltonians. When the counter-rotating terms can still be treated perturbatively, the system is in the pUSC regime. The system is in the pDSC regime when the interaction term cannot any more be treated as a perturbation, but is the main driver of the dynamics. However, in the pDSC regime, the qubit term ω_0 can be treated perturbatively. As emphasized in Ref. [69], this spectral classification is a qualitative classification and does not imply an abrupt change, but rather a gradual change in the physical properties of the QRM and the AsymQRM.

From Fig. 1 we infer that, in sharp contrast to the case of the QRM with $\epsilon = 0$, the entanglement entropy in the AsymQRM shows a number of resonance valleys in the npUSC-npDSC regime. Furthermore, the number of resonance valleys in this weak driving case is equal to $\lfloor (n-1)/2 \rfloor$ (where $\lfloor x \rfloor \equiv \{m \in \mathbb{Z} | m \leqslant x\}$) matching the number of energy-level crossing points in the original QRM [7,40]. Another remarkable difference of the AsymQRM is that the entanglement entropy in the pDSC regime decays to zero with the increase of the coupling strength g, while it remains 1 in the QRM.

The entanglement resonance signifies the efficient coupling of the relevant quantum states, which is essentially determined by the energy spectrum of the system. To understand the physical reason for the presence of the entanglement resonance in the npUSC-npDSC regime, we plot in Fig. 2 the corresponding energy spectrum of the AsymQRM. We can

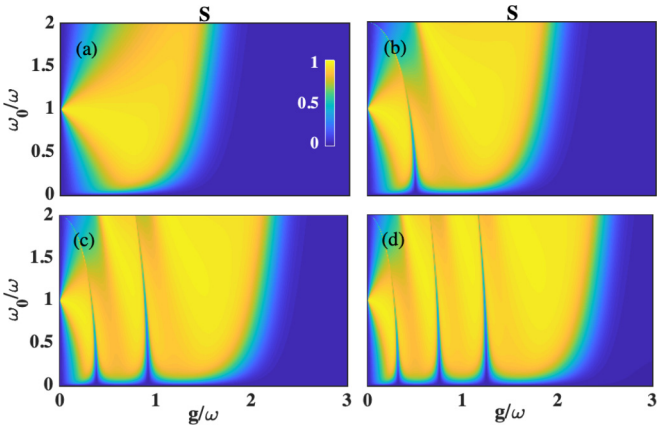

FIG. 3. Entanglement resonance of the eigenstates $|\Psi_n\rangle$ of the AsymQRM in the parameter plane of ω_0 and g when $n = 1$ in (a), $n = 3$ in (b), $n = 5$ in (c), and $n = 7$ in (d). We use $\epsilon = 0.1\omega$.

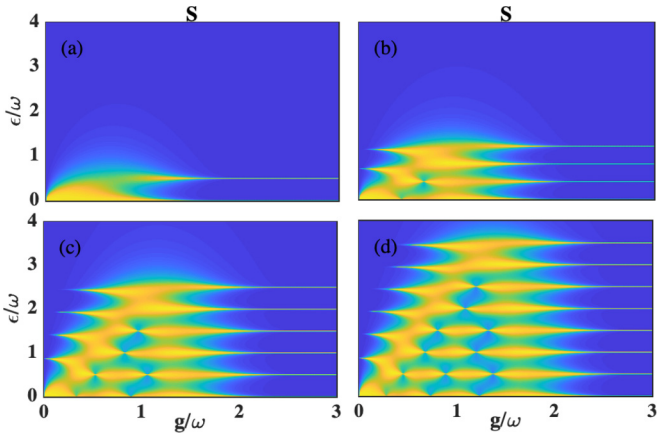

FIG. 4. Entanglement preservation of the eigenstates $|\Psi_n\rangle$ of the AsymQRM when $\epsilon = m\omega/2$ with $m \in \mathbb{Z}$. Here, $n = 2$ in (a), $n = 4$ in (b), $n = 6$ in (c), and $n = 8$ in (d).

see that all the energy-level crossings in the original QRM are opened by the static driving in the AsymQRM. It is interesting to find that the places of the avoided level crossings in Fig. 2 exactly match the ones of the entanglement resonances in Fig. 1. This can be physically understood as follows. The application of the static driving breaks the $\mathbb{Z}_2$ symmetry of the original QRM, which results in the opening of the energy-level crossings of the QRM. At the points of avoided level crossings, the high mixing of the two associated levels with different parities causes an abrupt change to the entanglement of the two involved quantum states.

To give a global picture of the entanglement resonance induced by the static driving, we plot in Fig. 3 the entanglement entropy in the plane ω_0 versus g for a chosen driving amplitude ϵ. It can be seen that the entanglement in the weak coupling limit is almost zero except for the resonance case $\omega_0 = \omega$. Then it changes to 1 with a tiny increase of g. With the further increase of g to the npUSC-npDSC regime, $\lfloor (n-1)/2 \rfloor$ entanglement resonance valleys appear. The entanglement in the small-ω_0 limit equals zero. It abruptly jumps to 1 with the increase of ω_0 except for the entanglement resonance position. Such resonance valleys become sharper and sharper with the increase of ω_0. Confirming the entanglement resonance induced by the avoided level crossing, this result suggests a useful way to understand the features of the energy spectra of the family of quantum Rabi models by monitoring the entanglement between the atom and the quantized field.

III. ENTANGLEMENT PRESERVATION IN THE pDSC REGIME

We have seen from Fig. 1 that the entanglement is not preserved in the pDSC regime when a static field is applied. Is this valid for arbitrary ϵ? To answer this question, we explore the entanglement property of the eigenstates $|\Psi_n\rangle$ of the AsymQRM for varying ϵ. In Fig. 4, we present the entanglement entropy of $|\Psi_n\rangle$ as a function of driving amplitude ϵ versus coupling strength g for $n = 2$, 4, 6, and 8 as examples (the results for other, even very large, values of n show the same physics). It is revealed that, besides the repeated resonance valleys in the npUSC-npDSC regime, which were analyzed in the last section, the entanglement in the pDSC regime also shows periodic resonance with increasing ϵ. Unlike the resonance valleys with increasing g in the npUSC-npDSC regime, the entanglement resonance with increasing ϵ in the pDSC regime shows periodic peaks. A maximal entanglement is observed in the pDSC regime at discrete values $\epsilon = m\omega/2$, with m being an integer. As ϵ further increases, the entanglement disappears again.

The appearance of the entanglement preservation in the pDSC regime when $\epsilon = m\omega/2$ is also caused by the avoided energy-level crossings. Taking $n = 8$ as an example, we plot in Fig. 5 the eighth eigenenergy and its nearest-neighbor energies as a function of ϵ when $g = 3\omega$. It is interesting to observe that the eighth energy level has eight avoided level crossings with its nearest-neighbor levels, which all occur at $\epsilon = m\omega/2$. These avoided level crossings correspond exactly with the entanglement preservation in Fig. 4(d). The result confirms that the entanglement preservation in the pDSC regime when $\epsilon = m\omega/2$ is essentially determined by the avoided level crossings.

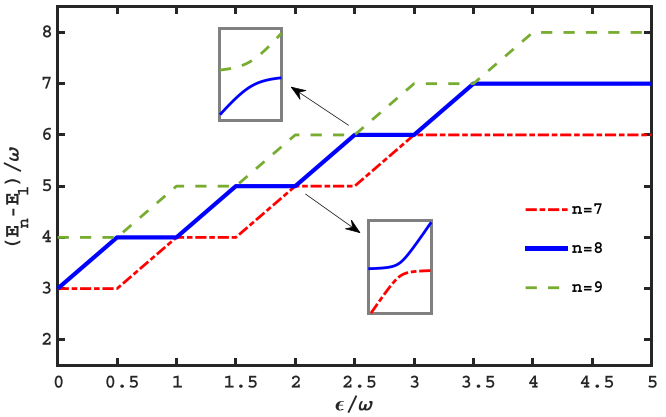

FIG. 5. Eigenenergies relative to the ground-state energy E_1 of the AsymQRM as a function of the driving amplitude ϵ in the pDSC regime when $g = 3\omega$. We use $\omega_0 = \omega$.

Governed by the $\mathbb{Z}_2$ symmetry, there are avoided level crossings, also called energy quasidegeneracies, in the QRM. It has therefore been unexpected to observe a restoration of the avoided level crossings also in the pDSC regime of the AsymQRM where the $\mathbb{Z}_2$ symmetry is broken. Actually, the reappearance of the energy quasidegeneracies in the AsymQRM is caused by a hidden symmetry of the AsymQRM [60–64] occurring when $\epsilon = m\omega/2$. Very recently, its symmetry operators for $m = 1$ and $m = 2$ were rigorously derived [63,65], and a general scheme to obtain the symmetry operators has been proposed [73]. Thus, in addition to the energy-spectrum features which have been investigated in previous work (see, e.g., Ref. [62]), the entanglement preservation in the pDSC regime revealed in this paper may serve as another piece of evidence of the hidden symmetry of the AsymQRM.

Another interesting behavior is that the entanglement preservation occurring at $\epsilon = m\omega/2$ only happens for a finite number of integers m. In order to obtain a physical understanding of this behavior, we apply the polaron picture [53–56]. This picture has been applied to a number of variants of the QRM. Rotating the Hamiltonian of Eq. (1) by the operator $e^{(i\pi/4)\sigma_y}$ to

$$\hat{H} = \epsilon\hat{\sigma}_z + \frac{\omega_0}{2}\hat{\sigma}_x + \omega\hat{a}^\dagger\hat{a} + g(\hat{a}^\dagger + \hat{a})\hat{\sigma}_z + \frac{\omega_0}{2} \tag{5}$$

and then expanding the Hamiltonian in the complete basis $\sum_{s_x=\pm}|s_x\rangle\langle s_x| = 1$ of $\hat{\sigma}_x \equiv \hat{\sigma}_+ + \hat{\sigma}_-$ and introducing the unit-mass coordinate $\hat{x} = (\hat{a} + \hat{a}^\dagger)/\sqrt{2\omega}$ and momentum operators $\hat{p} = i\sqrt{\omega/2}(\hat{a}^\dagger - \hat{a})$ of the quantized optical field [53,54], we can rewrite Eq. (1) as $\hat{H} = \hat{H}_0 + \hat{H}_1$ with

$$\hat{H}_0 = \sum_{s_x=\pm}\hat{h}_{s_x}|s_x\rangle\langle s_x| + \varepsilon_0, \tag{6}$$

$$\hat{H}_1 = \sum_{s_x=\pm}\frac{\omega_0}{2}|s_x\rangle\langle\bar{s}_x|, \tag{7}$$

where $\bar{s}_x$ means the flipped spin of s_x, $\varepsilon_0 = (\omega_0 - \omega)/2 - g^2/\omega$ is a constant energy, and $\hat{h}_{s_x} = \hat{p}^2/2 + \hat{V}_{s_x}$ with

$$\hat{V}_{s_x} = \frac{\omega^2}{2}\left(\hat{x} + x_{s_x}\right)^2 + s_x\epsilon \tag{8}$$

and $x_{s_x} = \sqrt{2\omega}s_x g/\omega^2$. Here, $\hat{V}_{s_x}$ are harmonic potentials with $s_x = \pm$ labeling the two $\hat{\sigma}_x$ eigenstates. In the pDSC regime, taking $\hat{H}_1$ as a perturbation, we obtain to leading order the eigenenergies of $\hat{H}$ as

$$E^{(0)}_{n,\pm} = n\omega \pm \epsilon. \tag{9}$$

As illustrated in Fig. 6, one can readily see how the driving ϵ affects the entanglement between the atom and the field. The dashed lines represent the case of $\epsilon = 0$, where $V_\pm$ are degenerate. With increasing ϵ, V_+ shifts upward and V_- shifts downward with the difference of their valleys being 2ϵ. The eigenenergies $E^{(0)}_{n,\pm}$ increase or decrease correspondingly. The second energy level $|2_-\rangle$ (take reference to the notation in Ref. [52]) in V_- crosses with the second energy level $|2_+\rangle$ and the first one $|1_+\rangle$ in V_+ when $\epsilon = 0$ and $\omega/2$, respectively. Except for these two values of ϵ, $|2_-\rangle$ has no chance to cross with the energy levels in V_- anymore. Due to the perturbation of $\hat{H}_1$, such energy-level crossings are reopened, which causes

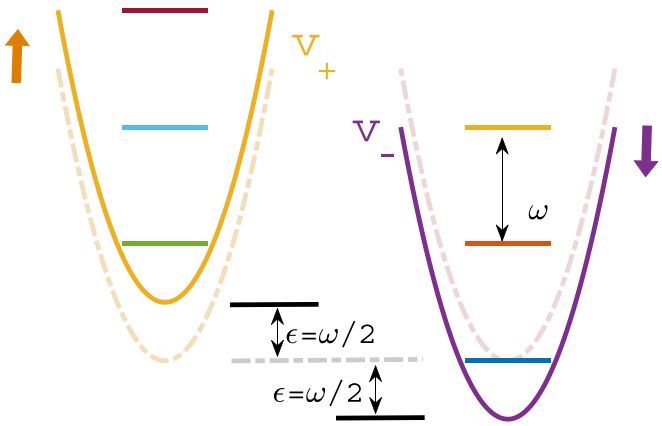

FIG. 6. Schematic diagram of the two harmonic potentials $V_\pm$ associated with the two $\hat{\sigma}_x$ eigenstates of $\hat{H}_0$. The static driving ϵ leads to the upward and downward shifts of V_+ and V_-, respectively. Here, $\epsilon = \omega/2$ is shown as an example.

a sufficient coupling of $|2_-\rangle$ with $|2_+\rangle$ and $|1_+\rangle$, respectively. This generates a large entanglement between the atom and the photon. It explains well the result in Fig. 4(a) that a finite entanglement for the second energy level is preserved in the pDSC regime only when $\epsilon = 0$ and $\omega/2$. In the same picture, the results in Figs. 4(b)–4(d) that the entanglement preservation occurs at $\epsilon = m\omega/2$ only for $m = 0, \ldots, n-1$ can be understood. Thus such a simple picture provides an intuitive explanation of the avoided level crossing and entanglement preservation in the pDSC regime.

IV. CONCLUSIONS

In summary, we have investigated the entanglement features in the eigenstates $|\Psi_n\rangle$ of the coupled system of a quantized optical field with a TLS subject to a statically driven two-level atom, i.e., the AsymQRM. The entanglement exhibits interesting features depending on the light-matter coupling strength and the driving amplitude, which are intrinsically related to the structure of the energy spectrum of the AsymQRM. We find that the entanglement shows $\lfloor(n-1)/2\rfloor$ resonance valleys with the change of the light-matter coupling strength in the npUSC-npDSC regime. Our results indicate that this is caused by the avoided level crossings induced by the static field. In the stronger pDSC regime, the entanglement exhibits resonance peaks at $\epsilon = m\omega/2$, with $m = 0, \ldots, n-1$. Our analysis demonstrates that such entanglement preservation is induced by the avoided level crossings due to the hidden symmetry of the AsymQRM. Our result is expected to be helpful to identify the features of the energy spectrum, such as the avoided energy-level crossings, and to further explore the related hidden symmetry properties of more theoretical models for light-matter interaction [67,74,75]. In addition, our method is promising to be applied to study quantum dot(s) with broken inversion symmetry in a cavity [76,77].

ACKNOWLEDGMENTS

We thank Prof. Jun-Hong An for helpful discussions. L.C. thanks Iñigo Arrazola for his useful comments. H.-P.E. thanks

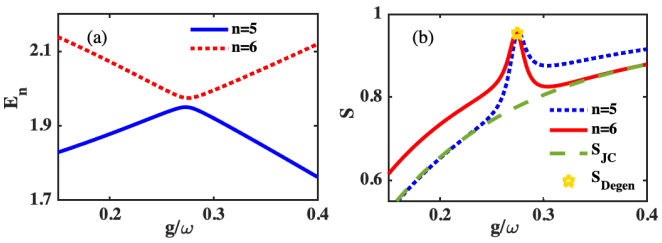

FIG. 7. (a) Avoided level crossing in the energy spectra of the JC model with external perturbation ϵ. (b) Entanglement entropy obtained by numerical (solid red line and dotted blue line) and degenerate perturbative (yellow star) methods. The entropy of the JC model (dashed green line) is also provided as a benchmark. $g/\omega = 0.2749$ is the point where the energies of the states $|1, +\rangle$ and $|2, -\rangle$ for the JC model become degenerate. $\omega_0 = 1.5\omega$ and $\epsilon = 0.05\omega$.

the School of Physical Science and Technology of Lanzhou University for their friendly and supportive hospitality. This work is supported by the International Postdoctoral Exchange Fellowship Program (Grant No. ZD202116) and the National Natural Science Foundation of Gansu Province, China (Grant No. 20JR5RA509).

APPENDIX: ENTANGLEMENT ENTROPY FOR THE ASYMMETRIC JAYNES-CUMMINGS MODEL

In order to provide a physical intuition for the appearance of the entanglement features in the AsymQRM, we apply a perturbation method to analytically study the entanglement entropy in the asymmetric quantum Jaynes-Cummings (AsymQJC) model, which is a model obtained from the AsymQRM after application of the rotating wave approximation [5] with the Hamiltonian

$$\hat{H}_{\text{AsymQJC}} = \frac{\omega_0}{2}\hat{\sigma}_z + \omega\hat{a}^\dagger\hat{a} + g(\hat{a}^\dagger\hat{\sigma}_- + \hat{a}\hat{\sigma}_+) + \epsilon\hat{\sigma}_x. \quad \text{(A1)}$$

The AsymQJC model shows entanglement resonance behavior similar to that of the AsymQRM. For instance, the energy-level crossings in the original quantum Jaynes-Cummings (JC) model are opened by the static driving in the AsymQJC model. The quantum JC model is exactly solvable, on the basis of which, by applying the degenerate perturbation method, we obtain the accurate value of the entropy for the peak of the entanglement resonance.

The opened energy gap is presented in Fig. 7(a), and the numerical and analytical results of the entropy are presented in Fig. 7(b). In Fig. 7(b), one can see that the analytical solution obtained by the degenerate perturbation method matches the numerical result perfectly. The fact that the entanglement is reduced (or increased) when there is a perturbation that removes a level crossing can be explained as a consequence of such a simple observation, i.e., if the unperturbed eigenstates are close to being maximally entangled, it is likely that their sum and difference are less entangled. In the same way, if the unperturbed eigenstates are close to being separable, their sum and difference are likely to be highly entangled. The detailed derivation is presented in the following section.

1. Analytical solution of the quantum Jaynes-Cummings model

In this section we summarize the analytical results for the quantum Jaynes-Cummings model [6]. The quantum Jaynes-Cummings model with Hamiltonian

$$\hat{H}_{\text{JC}} = \frac{\omega_0}{2}\hat{\sigma}_z + \omega\hat{a}^\dagger\hat{a} + g(\hat{a}^\dagger\hat{\sigma}_- + \hat{a}\hat{\sigma}_+) \quad \text{(A2)}$$

is known to be exactly solvable by elementary means. It conserves the total number operator $\hat{N} = \hat{a}^\dagger\hat{a} + \frac{1}{2}(1 + \hat{\sigma}_z)$.

For $N = 0$, the ground-state energy is $E_{0g} = -\frac{\omega_0}{2}$, and the eigenstate is denoted by $|g, 0\rangle$. The excitation energies and the excited states are given by

$$E_{n,\pm} = \left(n + \frac{1}{2}\right)\omega \pm \frac{\Omega}{2}, \quad n = 0, 1, 2, \ldots, \quad \text{(A3)}$$

where $\Omega = \sqrt{\Delta^2 + 4g^2(n+1)}$ and $\Delta = \omega_0 - \omega$, and

$$|n, +\rangle = C_n|n, e\rangle + D_n|n+1, g\rangle,$$
$$|n, -\rangle = D_n|n, e\rangle - C_n|n+1, g\rangle, \quad \text{(A4)}$$

where $C_n = \cos(\frac{\alpha_n}{2})$ and $D_n = \sin(\frac{\alpha_n}{2})$ with $\alpha_n = \tan^{-1}(\frac{2g\sqrt{n+1}}{\Delta})$.

2. Degenerate perturbation for the asymmetric quantum Jaynes-Cummings model

Turning on the static driving ϵ, the doubly degenerate energy-level crossing points of the original quantum JC model become avoided level crossings in the AsymQJC model. This is the reason we need to apply the degenerate perturbation method.

For the Hamiltonian of the quantum JC model at the degenerate point, i.e., for a particular value of g to be determined, the eigenvalue satisfies

$$\mathcal{E}_n^{(0)} = E_{n,+} = E_{n+1,-}, \quad \text{(A5)}$$

corresponding to two independent and orthogonal eigenfunctions $\phi_{n1} = |n, +\rangle$ and $\phi_{n2} = |n+1, -\rangle$,

$$\hat{H}_{\text{JC}}\phi_{ni} = \mathcal{E}_n^{(0)}\phi_{ni}, \quad i = 1, 2. \quad \text{(A6)}$$

This eigenvalue, $\mathcal{E}_n^{(0)}$, which is exact for the quantum JC model, now plays the role of the zeroth-order approximation eigenvalue for the asymmetric quantum JC model.

The corresponding zero-order wave function

$$\varphi_n^{(0)} = \sum_{i=1}^{2} c_i^{(0)}\phi_{ni}, \quad \text{(A7)}$$

where $c_i^{(0)}$ and the first-order energy eigenvalue $\mathcal{E}_n^{(1)}$ can be obtained by solving the eigenvalue equation

$$\sum_{j=1}^{2}\left(H'_{ij} - \mathcal{E}_n^{(1)}\delta_{ij}\right)c_j^{(0)} = 0, \quad i = 1, 2, \quad \text{(A8)}$$

where $H'_{ij} = \langle\phi_{ni}|\hat{H}'|\phi_{nj}\rangle$ represents the coupling between eigenstates ϕ_{ni} and ϕ_{nj} due to the operation of $\hat{H}' = \epsilon\sigma_x$. We obtain the first-order modifications of the degenerate eigenenergy

$$\mathcal{E}_{n,\pm}^{(1)} = \pm\epsilon D_n D_{n+1} \quad \text{(A9)}$$

as well as $c_1^{(0)} = \pm c_2^{(0)} = \frac{1}{\sqrt{2}}$ for the zeroth-order coefficients of the eigenstates.

Thus the total energy at the degenerate point is

$$E_{n,\pm} = \mathcal{E}_n^{(0)} + \mathcal{E}_{n,\pm}^{(1)}. \tag{A10}$$

The modified wave functions $\varphi_{n1}^{(0)}$ and $\varphi_{n2}^{(0)}$ are

$$\varphi_{n1}^{(0)} = \frac{1}{\sqrt{2}}(\phi_{n1} + \phi_{n2}), \quad \varphi_{n2}^{(0)} = \frac{1}{\sqrt{2}}(\phi_{n1} - \phi_{n2}). \tag{A11}$$

Note that the degeneracy of the quantum JC model is now lifted due to the asymmetry term $\epsilon\sigma_x$, and the level crossing at the degenerate point of the quantum JC model is now avoided for the asymmetric model.

Finally, we take the wave function $\varphi_{n1}^{(0)}$ as an example to calculate its corresponding entanglement entropy. It is known that the total density matrix is $\rho_{AB} = |\varphi_{n1}^{(0)}\rangle\langle\varphi_{n1}^{(0)}|$. One can get its reduced density matrix $\rho_A \equiv \mathrm{Tr}_B(\rho_{AB})$

$$\rho_A = \begin{pmatrix} D_{n+1}^2 + C_n^2 & D_n D_{n+1} \\ D_n D_{n+1} & D_n^2 + C_{n+1}^2 \end{pmatrix}. \tag{A12}$$

Now the von Neumann entropy S_{ρ_A} of the zero-level modified wave functions can be obtained:

$$S_{\rho_A} = -\mathrm{Tr}[\rho_A \log_2(\rho_A)]. \tag{A13}$$

As an example, we calculate the avoided level crossing corresponding to the intersection of states $|1, +\rangle$ and $|2, -\rangle$ in the JC model. The result is shown in Fig. 7. In the case of $\Delta = \omega_0 - \omega = 0.5\omega$ and $\epsilon = 0.05\omega$, the crossing point is at $g = 0.2749\omega$. Then, with the definition of α_n, C_n, and D_n [given below Eq. (A4)], one can calculate the reduced density matrix ρ_A and then the entropy S_{ρ_A}. Note that here the condition for which the perturbative method works, $\epsilon \ll \omega, \omega_0, g$, and the condition that the second-order terms are negligible should both be satisfied.

[1] S. Haroche and J.-M. Raimond, *Exploring the Quantum: Atoms, Cavities, and Photons* (Oxford University Press, Oxford, 2006).

[2] J. C. Garrison and R. Y. Chiao, *Quantum Optics* (Oxford University Press, Oxford, 2008).

[3] L. Allen and J. H. Eberly, *Optical Resonance and Two-Level Atoms* (Dover, Mineola, NY, 1987).

[4] I. I. Rabi, On the Process of Space Quantization, Phys. Rev. **49**, 324 (1936); Space Quantization in a Gyrating Magnetic Field, **51**, 652 (1937).

[5] E. T. Jaynes and F. W. Cummings, Comparison of quantum and semiclassical radiation theories with application to the beam maser, Proc. IEEE **51**, 89 (1963).

[6] H.-P. Eckle, Quantum Rabi model, in *Models of Quantum Matter: A First Course on Integrability and the Bethe Ansatz* (Oxford University Press, Oxford, 2019), Sec. 8.10, pp. 395–420.

[7] D. Braak, Integrability of the Rabi Model, Phys. Rev. Lett. **107**, 100401 (2011).

[8] Q.-H. Chen, C. Wang, S. He, T. Liu, and K.-L. Wang, Exact solvability of the quantum Rabi model using Bogoliubov operators, Phys. Rev. A **86**, 023822 (2012).

[9] L. Yu, S. Zhu, Q. Liang, G. Chen, and S. Jia, Analytical solutions for the Rabi model, Phys. Rev. A **86**, 015803 (2012).

[10] D. Braak, A generalized G-function for the quantum Rabi model, Ann. Phys. (Berlin) **525**, L23 (2013).

[11] D. Braak, Analytical solutions of basic models in quantum optics, in *Applications + Practical Conceptualization + Mathematics = Fruitful Innovation: Proceedings of the Forum of Mathematics for Industry 2014*, edited by R. S. Anderssen, P. Broadbridge, Y. Fukumoto, K. Kajiwara, T. Takagi, E. Verbitskiy, and M. Wakayama (Springer, New York, 2015), pp. 75–92.

[12] D. Braak, Symmetries in the Quantum Rabi model, Symmetry **11**, 1259 (2019).

[13] Q. Xie, H. Zhong, M. T. Batchelor, and C. Lee, The quantum Rabi model: solution and dynamics, J. Phys. A: Math. Theor. **50**, 113001 (2017).

[14] A. Le Boité, Theoretical methods for ultrastrong light-matter interactions, Adv. Quantum Technol. **3**, 1900140 (2020).

[15] J. Larson and T. Mavrogordatos, *The Jaynes-Cummings Model and Its Descendants* (IOP, London, 2021).

[16] I. Arrazola, Design of light-matter interactions for quantum technologies, arXiv:2101.11695 [quant-ph].

[17] A. Blais, A. L. Grimsmo, S. M. Girvin and A. Wallraff, Circuit quantum electrodynamics, Rev. Mod. Phys. **93**, 025005 (2021).

[18] D. Lv, S. An, Z. Liu, J.-N. Zhang, J. S. Pedernales, L. Lamata, E. Solano, and K. Kim, Quantum Simulation of the Quantum Rabi Model in a Trapped Ion, Phys. Rev. X **8**, 021027 (2018).

[19] M.-L. Cai, Z.-D. Liu, W.-D. Zhao, Y.-K. Wu, Q.-X. Mei, Y. Jiang, L. He, X. Zhang, Z.-C. Zhou, and L.-M. Duan, Observation of a quantum phase transition in the quantum Rabi model with a single trapped ion, Nat. Commun. **12**, 1126 (2021).

[20] G. Günter, A. A. Anappara, J. Hees, A. Sell, G. Biasiol, L. Sorba, S. De Liberato, C. Ciuti, A. Tredicucci, A. Leitenstorfer, and R. Huber, Sub-cycle switch-on of ultrastrong light-matter interaction, Nature (London) **458**, 178 (2009).

[21] T. Niemczyk, F. Deppe, H. Huebl, E. P. Menzel, F. Hocke, M. J. Schwarz, J. J. Garcia-Ripoll, D. Zueco, T. Hümmer, E. Solano, A. Marx, and R. Gross, Circuit quantum electrodynamics in the ultrastrong-coupling regime, Nat. Phys. **6**, 772 (2010).

[22] P. Forn-Díaz, J. Lisenfeld, D. Marcos, J. J. Garcia-Ripoll, E. Solano, C. J. P. M. Harmans, and J. E. Mooij, Observation of the Bloch-Siegert Shift in a Qubit-Oscillator System in the Ultrastrong Coupling Regime, Phys. Rev. Lett. **105**, 237001 (2010).

[23] F. Yoshihara, T. Fuse, S. Ashhab, K. Kakuyanagi, S. Saito, and K. Semba, Superconducting qubit-oscillator circuit beyond the ultrastrong-coupling regime, Nat. Phys. **13**, 44 (2017).

[24] J. Casanova, G. Romero, I. Lizuain, J. J. Garcia-Ripoll, and E. Solano, Deep Strong Coupling Regime of the Jaynes-Cummings Model, Phys. Rev. Lett. **105**, 263603 (2010).

[25] A. Crespi, S. Longhi, and R. Osellame, Photonic Realization of the Quantum Rabi Model, Phys. Rev. Lett. **108**, 163601 (2012).

[26] P. Forn-Díaz, L. Lamata, E. Rico, J. Kono, and E. Solano, Ultrastrong coupling regimes of light-matter interaction, Rev. Mod. Phys. **91**, 025005 (2019).

[27] M.-J. Hwang, R. Puebla, and M. B. Plenio, Quantum Phase Transition and Universal Dynamics in the Rabi Model, Phys. Rev. Lett. **115**, 180404 (2015).

[28] R. Puebla, M.-J. Hwang, J. Casanova, and M. B. Plenio, Probing the Dynamics of a Superradiant Quantum Phase Transition with a Single Trapped Ion, Phys. Rev. Lett. **118**, 073001 (2017).

[29] R. Puebla, M.-J. Hwang, and M. B. Plenio, Excited-state quantum phase transition in the Rabi model, Phys. Rev. A **94**, 023835 (2016).

[30] Z.-J. Ying, Symmetry-breaking patterns, tricriticalities, and quadruple points in the quantum Rabi model with bias and nonlinear interaction, Phys. Rev. A **103**, 063701 (2021); From quantum Rabi model to Janes-Cummings model: Symmetry-breaking quantum phase transitions, symmetry-protected topological transitions and multicriticality, Adv. Quantum Technol. **5**, 2100088 (2021).

[31] L. Garbe, M. Bina, A. Keller, M. G. A. Paris, and S. Felicetti, Critical Quantum Metrology with a Finite-Component Quantum Phase Transition, Phys. Rev. Lett. **124**, 120504 (2020).

[32] M. Nakahara and T. Ohmi, *Quantum Computing: From Linear Algebra to Physical Realizations* (CRC, Boca Raton, FL, 2008).

[33] J. Stolze and D. Suter, *Quantum Computing: A Short Course from Theory to Experiment*, 2nd ed. (Wiley-VCH, New York, 2008).

[34] M. A. Nielsen and I. L. Chuang, *Quantum Computation and Quantum Information*, 10th anniversary ed. (Cambridge University Press, Cambridge, 2010).

[35] A. D. Armour, M. P. Blencowe, and K. C. Schwab, Entanglement and Decoherence of a Micromechanical Resonator via Coupling to a Cooper-Pair Box, Phys. Rev. Lett. **88**, 148301 (2002).

[36] E. K. Irish and K. Schwab, Quantum measurement of a coupled nanomechanical resonator–Cooper-pair box system, Phys. Rev. B **68**, 155311 (2003).

[37] J. Larson, Integrability versus quantum thermalization, J. Phys. B: At. Mol. Opt. Phys. **46**, 224016 (2013).

[38] A. L. Grimsmo and S. Parkins, Cavity-QED simulation of qubit-oscillator dynamics in the ultrastrong-coupling regime, Phys. Rev. A **87**, 033814 (2013); Open Rabi model with ultrastrong coupling plus large dispersive-type nonlinearity: Nonclassical light via a tailored degeneracy, **89**, 033802 (2014).

[39] A. J. Maciejewski, M. Przybylska, and T. Stachowiak, Analytical method of spectra calculations in the Bargmann representation, Phys. Lett. A **378**, 3445 (2014); An exactly solvable system from quantum optics, **379**, 1503 (2015).

[40] H.-P. Eckle and H. Johannesson, A generalization of the quantum Rabi model: Exact solution and spectral structure, J. Phys. A: Math. Theor. **50**, 294004 (2017).

[41] Y.-F. Xie, L. Duan, and Q.-H. Chen, Quantum Rabi-Stark model: solutions and exotic energy spectra, J. Phys. A: Math. Theor. **52**, 245304 (2019).

[42] L. Cong, S. Felicetti, J. Casanova, L. Lamata, E. Solano, and I. Arrazola, Selective interactions in the quantum Rabi model, Phys. Rev. A **101**, 032350 (2020).

[43] H.-P. Eckle (unpublished).

[44] J. Dukelsky, S. Pittel, and G. Sierra, Exactly solvable Richardson-Gaudin models for many-body quantum systems, Rev. Mod. Phys. **76**, 643 (2004).

[45] M. Gaudin and J.-S. Caux, Various corollaries and extensions, in *The Bethe Wavefunction* (Cambridge University Press, Cambridge, 2014), Chap. 13, pp. 268–300.

[46] H.-P. Eckle, Quantum Tavis-Cummings model, in *Models of Quantum Matter: A First Course on Integrability and the Bethe Ansatz* (Oxford University Press, Oxford, 2019), Chap. 12, pp. 474–488.

[47] N. M. Bogoliubov, R. K. Bullough, and J. Timonen, Exact solution of generalized Tavis-Cummings models in quantum optics, J. Phys. A: Math. Gen. **29**, 6305 (1996).

[48] Q.-T. Xie, S. Cui, J.-P. Cao, L. Amico, and H. Fan, Anisotropic Rabi Model, Phys. Rev. X **4**, 021046 (2014).

[49] M. Tomka, O. El Araby, M. Pletyukhov, and M. Gritsev, Exceptional and regular spectra of a generalized Rabi model, Phys. Rev. A **90**, 063839 (2014).

[50] Y.-F. Xie, X.-Y. Chen, X.-F. Dong, and Q.-H. Chen, First-order and continuous quantum phase transitions in the anisotropic quantum Rabi-Stark model, Phys. Rev. A **101**, 053803 (2020).

[51] L. Cong and H.-P. Eckle (unpublished).

[52] G. Scala, K. Słowik, P. Facchi, S. Pascazio, and F. V. Pepe, Beyond the Rabi model: Light interactions with polar atomic systems in a cavity, Phys. Rev. A **104**, 013722 (2021).

[53] Z.-J. Ying, M. Liu, H.-G. Luo, H.-Q. Lin, and J. Q. You, Ground-state phase diagram of the quantum Rabi model, Phys. Rev. A **92**, 053823 (2015).

[54] L. Cong, X.-M. Sun, M. Liu, Z.-J. Ying, and H.-G. Luo, Frequency-renormalized multipolaron expansion for the quantum Rabi model, Phys. Rev. A **95**, 063803 (2017).

[55] L. Cong, X.-M. Sun, M. Liu, Z.-J. Ying, and H.-G. Luo, Polaron picture of the two-photon quantum Rabi model, Phys. Rev. A **99**, 013815 (2019).

[56] X. M. Sun, L. Cong, H.-P. Eckle, Z.-J. Ying, and H.-G. Luo, Application of the polaron picture in the two-qubit quantum Rabi model, Phys. Rev. A **101**, 063832 (2020).

[57] J. Audretsch, *Entangled Systems: New Directions in Quantum Physics* (Wiley, New York, 2008).

[58] *Quantum Information and Coherence*, edited by E. Andersson and P. Öhberg (Springer, New York, 2014).

[59] G. Cariolaro, *Quantum Communications* (Springer, New York, 2015).

[60] M. Wakayama, Symmetry of asymmetric quantum Rabi models, J. Phys. A: Math. Theor. **50**, 174001 (2017).

[61] J. Semple and M. Kollar, Asymptotic behaviour of observables in the asymmetric quantum Rabi model, J. Phys. A: Math. Theor. **51**, 044002 (2018).

[62] S. Ashhab, Attempt to find the hidden symmetry in the asymmetric quantum Rabi model, Phys. Rev. A **101**, 023808 (2020).

[63] V. V. Mangazeev, M. T. Batchelor, and V. V. Bazhanov, The hidden symmetry of the asymmetric quantum Rabi model, J. Phys. A: Math. Theor. **54**, 12LT01 (2021).

[64] Z.-M. Li and M. T. Batchelor, Hidden symmetry and tunneling dynamics in the asymmetric quantum Rabi model, Phys. Rev. A **103**, 023719 (2021).

[65] K. Kimoto, C. Reyes-Bustos, and M. Wakayama, Determinant expressions of constraint polynomials and the spectrum of the asymmetric quantum Rabi model, Int. Math. Res. Not. **2021**, 9458 (2021).

[66] Z.-M. Li, D. Ferri, D. Tilbrook, and M. T. Batchelor, General-

ized adiabatic approximation to the asymmetric quantum Rabi model: conical intersections and geometric phases, J. Phys. A: Math. Theor. **54**, 405201 (2021).

[67] Y. F. Xie and Q. H. Chen, Double degeneracy associated with hidden symmetries in the asymmetric two-photon Rabi model, Phys. Rev. Research **3**, 033057 (2021).

[68] S. Bose, A. Bayat, H. Johannesson, and P. Sodano, Entanglement content of many-body states via concurrence, negativity and Schmidt gap, in *Strongly Coupled Field Theories for Condensed Matter and Quantum Information Theory*, edited by A. Ferraz, K. S. Gupta, G. W. Semenoff, and P. Sodano (Springer, Cham, Switzerland, 2015), pp. 91–107.

[69] D. Z. Rossatto, C. J. Villas-Bôas, M. Sanz, and E. Solano, Spectral classification of coupling regimes in the quantum Rabi model, Phys. Rev. A **96**, 013849 (2017).

[70] M. Liu, Z.-J. Ying, J.-H. An, H.-G. Luo, and H.-Q. Lin, The asymmetric quantum Rabi model in the polaron picture, J. Phys. A: Math. Theor. **50**, 084003 (2017).

[71] J. Karthik, A. Sharma, and A. Lakshminarayan, Entanglement, avoided crossings, and quantum chaos in the Ising model with a tilted magnetic field, Phys. Rev. A **75**, 022304 (2007).

[72] S. Sauer, F. Mintert, C. Gneiting, and A. Buchleitner, Entanglement resonances of driven multi-partite quantum systems, J. Phys. B: At. Mol. Opt. Phys. **45**, 154011 (2012).

[73] Y.-F. Xie and Q.-H. Chen, General symmetry operators of the asymmetric quantum Rabi model within Bogoliubov operator approach, J. Phys. A: Math. Theor. **55**, 225306 (2022).

[74] X. Lu, Z.-M. Li, V. V. Mangazeev, and M. T. Batchelor, Hidden symmetry operators for asymmetric generalised quantum Rabi models, Chin. Phys. B **31**, 014210 (2022).

[75] X. Lu, Z.-M. Li, V. V. Mangazeev, and M. T. Batchelor, Hidden symmetry in the biased Dicke model, J. Phys. A: Math. Theor. **54**, 325202 (2021).

[76] O. V. Kibis, G. Ya. Slepyan, S. A. Maksimenko, and A. Hoffmann, Matter Coupling to Strong Electromagnetic Fields in Two-Level Quantum Systems with Broken Inversion Symmetry, Phys. Rev. Lett. **102**, 023601 (2009).

[77] I. G. Savenko, O. V. Kibis, and I. A. Shelykh, Asymmetric quantum dot in a microcavity as a nonlinear optical element, Phys. Rev. A **85**, 053818 (2012).